Moment canting in amorphous FeSiB ribbons in applied fields: unpolarized Mossbauer effect studies

Moment canting in amorphous FeSiB ribbons in applied fields: unpolarized Mössbauer effect studies

Q A Pankhurst†, J Z Jiang†‖, S Betteridge‡, M R J Gibbs§ and
G A Gehring§

† Department of Physics and Astronomy, University College London, London WC1E 6BT, UK
‡ Department of Physics, University of Liverpool, Liverpool L69 3BX, UK
§ Department of Physics, University of Sheffield, Sheffield S3 7RH, UK

Abstract. The phenomenon of 'moment canting', where the atomic moments in a soft magnetic material do not completely align with an applied field of substantial magnitude, has been measured as a function of field in field annealed $Fe_{78}Si_9B_{13}$ metallic glass ribbons. Probability distributions for the Fe moment directions were deduced from unpolarized ^{57}Fe Mössbauer experiments. A method of analysis was devised to account for spectral saturation effects, and validated with reference to polycrystalline α-Fe. Fields of up to 0.5 T were applied at room temperature in the ribbon plane. Even in 0.5 T the in-plane moment canting did not fall to zero, with the standard deviation of the Gaussian spread in moment directions remaining at $12° \pm 1°$. Fields of up to 9 T were applied at 4.2 K, normal to the ribbon plane. Even in 9 T appreciable canting was observed, with a Gaussian standard deviation of $11° \pm 1°$ with respect to the applied field direction. An *a priori* 'combed hair' model was developed to describe the moment canting that would result from the presence of a few frustrated exchange interactions between some magnetic atoms. Long-distance moment canting was predicted, with a truncated inverse sine probability distribution. The data were found to be adequately described using this model.

1. Introduction

The issue of moment canting in metallic glasses is of considerable interest from a fundamental viewpoint, and also with respect to the applicability of these materials in modern transducer and sensor devices. Over the last few years a body of evidence has been amassed from polarized neutron scattering [1, 2], magnetostriction [3, 4], high-field magnetization [5], and Mössbauer spectroscopy [6–8] experiments which supports the conclusion that in some nominally ferromagnetic amorphous alloys the atomic moments are not collinear in the presence of an applied field. The most surprising aspect of this non-collinear state is that it appears to persist in applied fields well in excess of the technical saturation field of the alloys concerned. An example of this is the metallic glass $Fe_{78}Si_9B_{13}$, which has a technical saturation field at room temperature of the order of 25 mT, but which shows a continuing increase in magnetization, and therefore a lack of absolute saturation, even in pulsed magnetic fields as high as 120 T [5].

The observation of moment canting effects in such large fields indicates that the determining factors are related to the strong exchange interactions between magnetic ions. In the last few years several authors have considered theoretical and numerical models

‖ Present address: Physics Department, Technical University of Denmark, DK-2800 Lyngby, Denmark.

aimed at establishing the mechanics of the moment canting [9–12], as well as the nature of the magnetic ground state of these alloys [13, 14], based on some sort of exchange-mediated behaviour. Most of these models postulate that the local exchange experienced by the atomic moments can vary in both magnitude and sign, and that as a consequence the moment correlation length can be drastically reduced in localized regions in the material.

To date there have been few studies of moment canting which have made quantitative, as well as qualitative, assessments of the systematic applied-field-dependent characteristics of the moment canting. This is the goal of our work. We report here on unpolarized Mössbauer effect measurements, and later we will report on polarized Mössbauer effect measurements [15]. The experimental results will be discussed with reference to a disturbed exchange model of moment canting which extends earlier theoretical concepts to provide a new quantitative description for the shape of the moment canting probability distribution.

In this paper we describe a systematic series of measurements using Mössbauer spectroscopy to probe the atomic moment distributions in post-production treated $Fe_{78}Si_9B_{13}$ ribbons. We describe the results of experiments in two distinct geometries: one with moderate fields (up to 500 mT) applied in-plane, and a second with large fields (up to 9 T) applied normal to the plane. The validity and limitations of the unpolarized Mössbauer technique for the measurement of moment canting is critically assessed and discussed. A new 'combed hair' disturbed exchange model of moment canting is presented, and experimentally observable quantities derived. These are then compared with the measured data, and conclusions drawn regarding the nature of moment canting in $Fe_{78}Si_9B_{13}$.

2. Experimental details

2.1. Sample preparation

The $Fe_{78}Si_9B_{13}$ samples in this study were cut from a 25 μm thick roll of commercially available source material, METGLAS® 2605-S2. Data were recorded from samples in either their 'as received' state, or in the post-production treated 'stress relieved' or 'field annealed' states. Details of the specimen dimensions and post-production treatments are given in table 1. Since throughout this paper we will refer, wherever relevant, to previous work on these $Fe_{78}Si_9B_{13}$ ribbon specimens [8, 16–20], details of the full range of related samples are included in table 1.

Details of the field annealing processes are as follows. First the individual samples were sandwiched between a pair of flat-faced aluminium plates and placed between the poles of a four inch electromagnet. The magnetic field was then applied, and the samples heated using a hot-air gun. Temperatures were monitored from a thermocouple attached to one of the plates. The plates were heated to 400 °C (within $\sim$ 3.5 min), and held constant within ±1 °C throughout the anneal. After a fixed time period, the hot-air gun heater was turned off, but the fan left on. The plate temperature fell below 100 °C within four minutes. The field was left on until the plate temperature dropped below 60 °C. The rectangular samples were aligned by eye, within an accuracy of about ±2 °, with either their long axis (defined as the x axis) or their short axis, (the y axis) parallel to the applied field. Stress relieved samples were prepared in the same manner, except that no field was applied during the heating and cooling cycle.

For each set of samples, x-ray diffraction data were recorded from those that were annealed for the longest time. Although we know from previous work that prolonged annealing can give rise to the formation of surface crystallites, in none of the samples discussed in this paper was there any evidence of crystallization.

Table 1. Dimensions and post-production treatment details for the $Fe_{78}Si_9B_{13}$ ribbon samples used in this work and in relevant earlier work by the authors. Unless otherwise specified, the samples were rectangular in shape. Abbreviations: AR for as-received, SR for stress relieved, FA-*x* for field annealed along the long *x* axis of the sample, and FA-*y* for field annealed along the short *y* axis of the sample.

Sample	Dimensions	Treatment	Reference
1	45 mm×25 mm	AR	[17, 19]
2	45 mm×25 mm	SR: 400 °C, 40 min	[17, 19]
3	45 mm×25 mm	FA-*x*: 0.4 T, 400 °C, 40 min	[17–19]
4	45 mm×25 mm	FA-*y*: 0.4 T, 400 °C, 40 min	[17, 19]
5	35 mm×17.5 mm	SR: 400 °C, 40 min	[15]
6	35 mm×17.5 mm	FA-*x*: 0.4 T, 400 °C, 60 min[a]	[8, 15]
7	35 mm×25 mm	SR: 400 °C, 20 min	[20]
8	35 mm×25 mm	FA-*x*: 0.4 T, 400 °C, 10 min	[20]
9	35 mm×25 mm	FA-*x*: 0.4 T, 400 °C, 20 min	This work + [20]
10	35 mm×25 mm	FA-*x*: 0.4 T, 400 °C, 60 min	[20]
11	19 mm diameter disc	FA: 0.4 T, 400 °C, 20 min	This work

[a] There is a typographical error in [8] relating to the duration of the anneal.

2.2. *Mössbauer experiments*

Mössbauer spectra were recorded using a 100 mCi unpolarized single-line ^{57}CoRh source of 14.4 keV ^{57}Fe γ-rays. A constant acceleration mode of operation was used, with the source velocity following a triangular drive waveform. Spectra were recorded with a 576 channel multi-channel analyser, and the spectra were folded to remove baseline curvature. Calibration between channel and source velocity was with reference to an α-Fe foil at room temperature. Each spectrum took approximately 24 h to collect.

The measurement of moment distributions in Fe-based metallic glass ribbons using ^{57}Fe Mössbauer spectroscopy is relatively straightforward. In a six-line ^{57}Fe Mössbauer spectrum obtained from a magnetically ordered material, the relative area of the outer:middle:inner pairs of lines fall in the ratio 3:*r*:1, where *r* depends on the angle α between the absorbing Fe atom's moment μ, and the propagation direction of the γ-ray beam (see figure 1). This variation in *r* originates from the angular probability distributions of the radiative transitions between the Fe atom's nuclear sub-levels. In a metallic glass such as $Fe_{78}Si_9B_{13}$, there is a distribution of moment directions, and therefore a distribution of contributions to *r*. It can be shown that

$$r = 4\langle \sin^2 \alpha \rangle / (1 + \langle \cos^2 \alpha \rangle) \tag{1}$$

where the angular brackets refer to the spatial averages of $\sin^2 \alpha$ and $\cos^2 \alpha$. From any single Mössbauer spectrum one can determine a value for the spatially averaged angle $\langle \alpha \rangle$, but if detailed information about the distribution of moment directions is required it is advisable to record a series of spectra, and analyse *r* as a function of the angle of incidence of the γ-ray beam [16].

For the in-plane applied field experiments described in section 3 a variable angle geometry was employed, where the angle of incidence, ψ, between the γ-ray beam and the normal to the ribbon plane was systematically varied. The variable angle geometry is shown in figure 1, which defines a co-ordinate system in which the *x* axis is parallel to the long axis of the ribbon, the *y* axis is along the width, and the *z* axis is the normal to the ribbon plane. For each sample spectra were recorded for γ-ray propagation directions of $\psi = 0°, 20°, 40°$ and $60°$ in both the *xz* and *yz* planes: a total of seven different spectra for
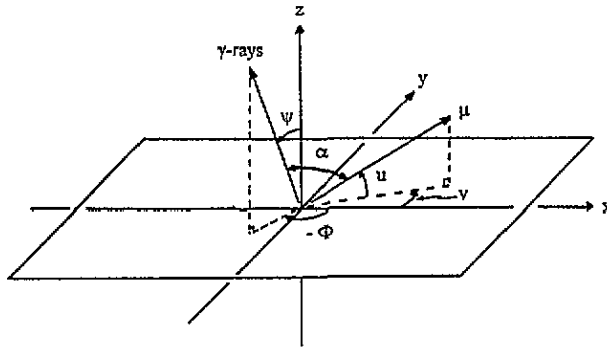
Figure 1. The experimental geometry for the Mössbauer experiments, showing the angle ψ between the incident γ-ray beam and the normal to the ribbon plane (the z axis). Also defined are the out-of-plane and in-plane polar angles u and v for any given atomic moment μ, and the angle α between μ and the γ-ray beam.

each sample. The variation in ψ was achieved by mounting the ribbons on a swivel plate which was free to rotate about an axis perpendicular to the γ-ray beam. The ribbons were mounted by sandwiching them between a lead mask (with a hole to allow the transmission of the γ-rays) and a perspex plate, taking care to minimize the possible application of stress to the sample.

2.3. Applied-field geometrics

Two different applied field sources and geometries were employed: an electromagnet for in-ribbon-plane fields of up to 500 mT, and a superconducting magnet for fields of up to 9 T directed normal to the ribbon plane.
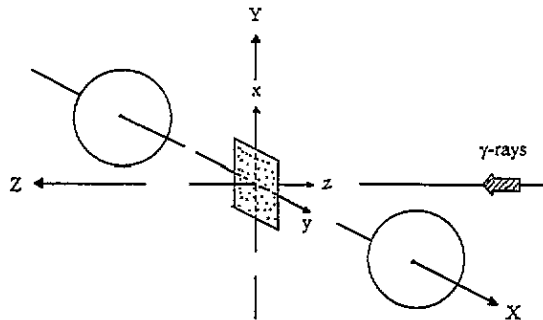

Figure 2. A schematic diagram of the positioning of the rectangular FeSiB ribbon sample between the poles of a four inch electromagnet relative to the direction of propagation of the Mössbauer γ-rays. Two series of spectra were recorded, both with the ribbon z axis at 0°, 20°, 40° and 60° to the Z axis. In the first series the ribbon y axis was kept parallel to the applied field (the X axis) and the ribbon x axis was rotated in the YZ plane. In the second series the ribbon x axis was vertical (parallel to the Y axis) and the ribbon y axis was rotated in the XZ plane.

In-plane fields of 7 mT, 50 mT and 500 mT were applied to the ribbons using a four inch electromagnet. A laboratory reference co-ordinate system is defined in figure 2, where the X axis is horizontal and along the pole axis of the electromagnet, the Y axis is vertical, and the Z axis is horizontal and along the γ-ray beam. As the purpose of the experiment was to observe the effect of an applied field directed perpendicular to the magnetic anisotropy

induced by the anneal field (along the long axis of the ribbon, the x axis), the applied field was directed as near as possible to the y axis. This was achieved exactly for the spectra recorded with ψ in the xz plane: by placing the ribbon in the electromagnet with its y axis parallel to the X axis, the ribbon could be rotated about the y axis, with its x direction moving in the YZ plane (see figure 2). However, for ψ varying in the yz plane, the x axis was kept parallel to the Y axis, and the ribbon rotated about the x axis. Although this successfully allowed the y direction to move in the XZ plane, it meant that the applied field direction could no longer be assumed to be in-plane with respect to the ribbon. This point will be discussed further in section 3, where it is shown that the high permeability of the ribbons acts to moderate the applied field directions. This keeps the lines of magnetic flux within the ribbon plane for the small 7 mT and 50 mT applied fields, although this is no longer true for the 500 mT field.

For the normal-to-plane applied field experiments a 19 mm diameter disc was used. This disc was placed in a stress-free plastic sample holder, and mounted in the centre of a 10 T superconducting solenoid. The ribbon was completely immersed in liquid helium, and the applied field and γ-rays were directed along the normal to the ribbon plane.

subsectionThe fitting procedure To derive the distribution of moment directions in a metallic glass ribbon from its Mössbauer spectra, an appropriate fitting procedure must be adopted. There are two main issues: (i) how to model the distribution in the Fe magnetic hyperfine fields and incorporate the effect of non-zero electric quadrupole interactions, and (ii) how to cope with any saturation effects that may be present.

The Mössbauer spectra of $Fe_{78}S_9B_{13}$ (see figure 3) have broad absorption lines due to the distribution in magnitude of the magnetic hyperfine field present at the ^{57}Fe nuclei. The magnitude of the hyperfine splitting reflects both the core electron polarization due to the valence and conduction band electrons and the dipolar field contributions from neighbouring magnetic atoms. The distribution of hyperfine fields, evident in the broad lines, results from the variation in local environments experienced by the Fe atoms in the glassy alloy.

The manner in which one models this distribution in hyperfine fields (known colloquially as the 'P(H) distribution') depends both on the system being studied, and the degree of accuracy sought. One approach is to use a spectral lineshape that reflects the P(H) distribution, as in the 'Pearson VII' model [21]. This model takes full account of quadrupole interactions, no matter how large. It has the advantage of simplicity, but provides little information on the P(H) distribution. There are two common methods for P(H) measurements, the Window [22] and Hesse and Rübartsch [23] methods. Both make no *a priori* assumptions about the nature of the distributions, and both assume that the effect of any non-zero quadrupole interactions are small compared to the magnetic dipole interactions. In many cases these are appropriate and advantageous assumptions, although there are sometimes problems that arise due to the relatively unconstrained nature of the analysis.

A fourth method of modelling the P(H) distribution is the Lines and Eibschütz method [24]. In this model the spectra are fitted using six Voigtian line profiles (Gaussian distributions of Lorentzian lines) whose positions are constrained to be physically realizable. The model incorporates experimentally fitted correlations between the electric monopole, electric quadrupole and magnetic hyperfine parameters of the sample, making it more realistic than either the Window or the Hesse and Rübartsch models. It should be noted however that the Lines and Eibschütz model is most appropriate in materials where the quadrupole interaction is small compared to the magnetic splitting, and the spectral lines are well separated from each other. This condition is satisfied in $Fe_{78}Si_9B_{13}$. Also, there is an inherent assumption in the model that the P(H) distribution may be adequately described
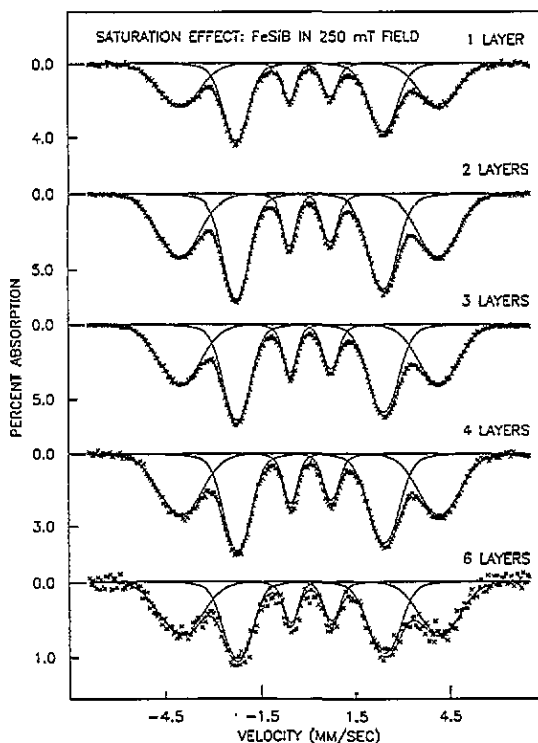
Figure 3. The room temperature Mössbauer spectra of as-cast $Fe_{78}Si_9B_{13}$ ribbons (sample 1) in an in-plane applied field of 250 mT. The differences in the spectra observed as a function of the number of layers, each 25 μm thick, stacked upon each other, are indicative of thickness saturation effects. The solid lines result from a least-squares fit using a constrained set of six Voigtian line profiles.

by a single-mode Gaussian distribution, and that there are no significant contributions from e.g. low-field tails in the $P(H)$ distribution.

The question of whether a single-mode $P(H)$ distribution is a reasonable model for $Fe_{78}Si_9B_{13}$ requires consideration. In the 1980s there was some debate in the literature following a report that $Fe_{78}Si_9B_{13}$ possessed a bi-modal $P(H)$ distribution [25]. This conclusion was challenged and shown to be attributable to artefacts associated with the Window method of $P(H)$ analysis [26]. It was also argued that in a material such as $Fe_{78}Si_9B_{13}$, with only one transition metal present, there was no reason to expect any bi-modality in the distribution [26]. To our knowledge there have been no further reports of any low-field contributions of bi-modality in the $P(H)$ distribution of $Fe_{78}Si_9B_{13}$.

Nevertheless, we have tested this issue further by using a variation of the spectral subtraction method of Vincze [27]. Two independent spectra were recorded in zero applied field on a sample of field annealed $Fe_{78}Si_9B_{13}$. The only difference between the two spectra was that in one case the γ-ray beam was inclined at an angle $\psi = 40°$ in the xz plane, and in the other case it was at $\psi = 40°$ in the yz plane. The spectra differed only in the relative areas of their second and fifth lines in accordance with equation (1). By scaling the counts in one spectrum relative to the other, and then subtracting them, it is possible to obtain a spectrum that reveals the shape of the second and fifth lines on their own. This is shown in figure 4. If there were any significant bi-modality or low-field contributions in

the $P(H)$ distribution, this would be evidenced by asymmetric or double-peaked lineshapes in the subtracted spectrum. It is clear in figure 4 that this is not the case. We therefore conclude that the $P(H)$ distribution in $Fe_{78}Si_9B_{13}$ is adequately described as a single-mode Gaussian distribution, and in the remainder of this work we have chosen to use the Lines and Eibschütz fitting procedure.
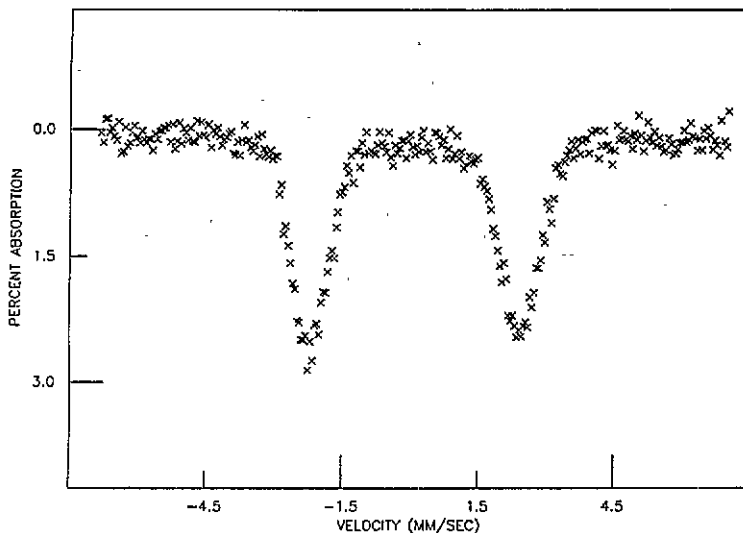

Figure 4. Difference spectrum obtained by subtracting two room temperature Mössbauer spectra of a field annealed ribbon of $Fe_{78}Si_9B_{13}$ from each other. The two spectra were recorded in zero applied field, with the incident γ-ray beam oriented at 40° to the normal to the ribbon, in the xz and yz planes respectively. The difference spectrum shows only the second and fifth lines of the hyperfine sextet, the areas of which respond to the distribution in moment directions. The smooth shape of the lines reveals that the $P(H)$ distribution in hyperfine fields in $Fe_{78}Si_9B_{13}$ has a single mode, with no significant bi-modality or low-field tail.

It may be noted in passing that the variation of the spectra subtraction method described here is new, and that it overcomes some of the strongest criticisms of Vincze's method that have been raised in the past [28]. Specifically, it does not rely on comparing the data from zero field and applied field runs, and therefore does not require that all the magnetic moments in the sample are equally affected by the applied field. Another advantage is that the two spectra used both had the same γ-ray inclination angle and therefore were of the same effective thickness. As discussed below, this means that saturation effects were equivalent for the two spectra used in the subtraction.

2.4. Correction for saturation effects

A series of Mössbauer spectra obtained for 1, 2, 3, 4 and 6 layers of as-cast $Fe_{78}Si_9B_{13}$ ribbon (sample 1) are shown in figure 3. The ribbons were subject to an in-plane field of 250 mT from a pair of NdFeB permanent magnets mounted on a rectangular steel frame, and the γ-ray beam was directed normal to the ribbon plane. Given that 250 mT is an order of magnitude greater than the technical saturation field of $Fe_{78}Si_9B_{13}$, one would expect that the atomic Fe moments would lie close to the applied field. However, there are substantial casting stresses in as-cast ribbons, which lead to significant out-of-plane canting [17]. In the spectra in figure 3 the angle $\langle\alpha\rangle$ in equation (1) is $\sim 77°$, with an area ratio 3:3.6:1 in

the outer:middle:inner pairs of lines. As the thickness of the absorber increases the areas of the lines become more equal. This is due to saturation. As the number of layers of ribbon increases, the sample becomes so 'thick' that the most intense absorption lines saturate as all the γ-rays corresponding to that energy are absorbed. The relative intensity of the less probable nuclear transitions (e.g. the central two absorption lines) then appear to have an enhanced absorption relative to the most intense lines.

A number of methods of varying complexity have been proposed to model saturation effects. The most rigorous is the 'transmission integral' method [29, 30], where the saturation effects are incorporated into the underlying description of the shape and area of the absorption lines. However, this is a somewhat cumbersome approach, especially when dealing with spectra containing distributions of hyperfine parameters. A simpler, first-order approach is that of Shirley et al [31], which in essence is a phenomenological model of the effect of saturation, rather than the first-principles approach of the transmission integral. In the Shirley et al model the sample is assigned an 'effective thickness' parameter, τ_A. The increased linewidth of the observed absorption lines is then approximated by

$$\Gamma = \Gamma_0(1 + 0.135\tau_A) \tag{2}$$

for $0 < \tau_A < 5$, where Γ_0 is the natural linewidth for an ideally thin absorber. Similarly the reduced area of the absorption lines is approximated by

$$A = 2A_0(1 + 0.135\tau_A)[1 - \exp(-\tfrac{1}{2}\tau_A^2)I_0(\tfrac{1}{2}\tau_A)]/\tau_A \tag{3}$$

for $0 < \tau_A < 5$, where $I_0(\tfrac{1}{2}\tau_A) = J_0(\tfrac{1}{2}i\tau_A)$ is the zeroth-order Bessel function of imaginary argument evaluated at $\tfrac{1}{2}\tau_A$ [31].

The spectra in figure 3 were least-squares fitted using a computer program based on the Lines and Eibschütz $P(H)$ model, incorporating Shirley et al corrections for saturation effects. Each Voigtian profile was approximated by a Gaussian probability distribution of natural linewidth Lorentzian lines, with neighbouring Lorentzians separated by 0.04 mm s^{-1}. All five spectra were simultaneously fitted so that the hyperfine parameters controlling the Voigt profiles in each spectrum were identical. A global thickness parameter τ_A was fitted, and was scaled according to the number of ribbon layers for each spectrum: e.g. the effective thickness of the single-layer spectrum was τ_A', while that of the six-layer spectrum was $6\tau_A'$. The thickness was also scaled for each constituent Lorentzian line in the Voigt profile, so that each Lorentzian had a specific τ_A value, appropriate for use in equations (2) and (3), associated with it. The best fit to the data yielded a global thickness parameter value of $\tau_A' = 33.5$, which corresponds to a maximum thickness for an individual Lorentzian line of $\tau_A^{max} = 2.4$, which occurred for the six-layer spectrum. This is well within the validity limits of the Shirley et al approximations. It is evident from the high quality of the fit (the solid lines in figure 3) that the model is sufficiently flexible to describe the observed data.

2.5. A double Gaussian model for the distribution in Fe moment direction

From our earlier studies on the moment distributions in Fe$_{78}$Si$_9$B$_{13}$, we have concluded that an appropriate and physically realistic model for the distribution of moment direction is a double Gaussian [19]. In this model the probability distribution is expressed as

$$P(u, v) = [1/(2\pi\sigma_u\sigma_v)] \exp\{-[(u - u_0)^2/2\sigma_u^2] - [(v - v_0)^2/2\sigma_v^2]\} \tag{4}$$

where u and v are the out-of-plane and in-plane polar angles defining the directions of each individual moment (see figure 1), and σ_u and σ_v are the Gaussian standard deviations defining the spread in the orientation angles. The probability distribution is taken to be centred on the direction (u_0, v_0).

By monitoring the Mössbauer area parameter r as a function of the polar and azimuthal angles of incidence of the incoming γ-rays, ψ and Φ, it is possible to uniquely determine the parameters u_0, v_0, σ_u and σ_v for the probability distribution [19]. For the coordinate system shown in figure 1

$$\sin^2 \alpha = 1 - \cos^2 u \sin^2 \psi (\cos v \cos \Phi + \sin v \sin \Phi)^2 - \sin^2 u \cos^2 \psi$$
$$- \tfrac{1}{2} \sin 2u \sin 2\psi (\cos v \cos \Phi + \sin v \sin \Phi) \tag{5}$$

from which the spatial average may be expressed as

$$\langle \sin^2 \alpha \rangle = \int_{-\pi}^{+\pi} \int_{-\pi/2}^{+\pi/2} P(u, v) \sin^2 \alpha \cos u \, \mathrm{d}u \, \mathrm{d}v \tag{6}$$

where $\mathrm{d}\Omega = \cos u \, \mathrm{d}u \, \mathrm{d}v$ is the surface element in a unit sphere. It has proved to be straightforward to write a computer program to numerically integrate equations (6) using algorithms from the NAG subroutine library. An alternative means of solving the equations has also been tested, where an equi-probable two-dimensional net in u and v is used. This method involves the one-dimensional integration, in u and v respectively, of the Gaussian distribution in equation (4) to obtain solutions involving the error function. Comparisons have been made between the two programs, and agreement within $\pm 1\%$ has been achieved using a 500×500 two-dimensional grid for the equi-probability method.

3. Response to in-plane fields up to 0.5 T

3.1. Control experiment in α-Fe

Before considering the applied-field data for the $Fe_{78}Si_9B_{13}$ samples, it is instructive to first test the fitting procedure outlined above on a relatively well-known system. For this purpose we chose a 25 μm thick foil of pure polycrystalline α-Fe. Mössbauer spectra were recorded with the foil mounted in the 250 mT permanent magnet frame. Representative spectra are shown in figure 5. The spectra were fitted using Voigt profiles, including saturation effects. The results obtained for the area ratio parameter r are shown in figure 6. These data were then analysed using the double Gaussian moment distribution model. The parameters obtained indicate that the moments were distributed about the applied field direction, with an out-of-plane standard deviation $\sigma_u = 6.0° \pm 0.4°$ and an in-plane standard deviation $\sigma_v = 9.4° \pm 0.6°$.

These are realistic results for polycrystalline α-Fe. The magnetocrystalline anisotropy in α-Fe is rather large, $K_1 \sim 5 \times 10^4$ J m^{-3}, and on the basis of this alone one expects a mean angle between the 250 mT field and the Fe moments $\sim 2.5°$ [32], corresponding to a Gaussian standard deviation $\sim 2°$. Adding the effect of any remanent internal stresses or impurity pinning centres, it is reasonable to expect that the moment distribution would have standard deviations of the order of those measured. In earlier polarized Mössbauer measurements on in-plane moment distributions in stress relieved α-Fe we measured a mean angle between a 250 mT field and the Fe moments $\sim 6°$, corresponding to a Gaussian deviation $\sim 4.5°$ [8]. The slightly higher values obtained here may be attributed to the different histories of the α-Fe samples used.

3.2. FeSiB experiments

In earlier experiments on $Fe_{78}Si_9B_{13}$ ribbons we have found that post-production treatment has a major effect on the zero-field moment distribution [17, 19, 20]. For this work we have therefore chosen to concentrate on a well-characterized field annealed ribbon, one that was
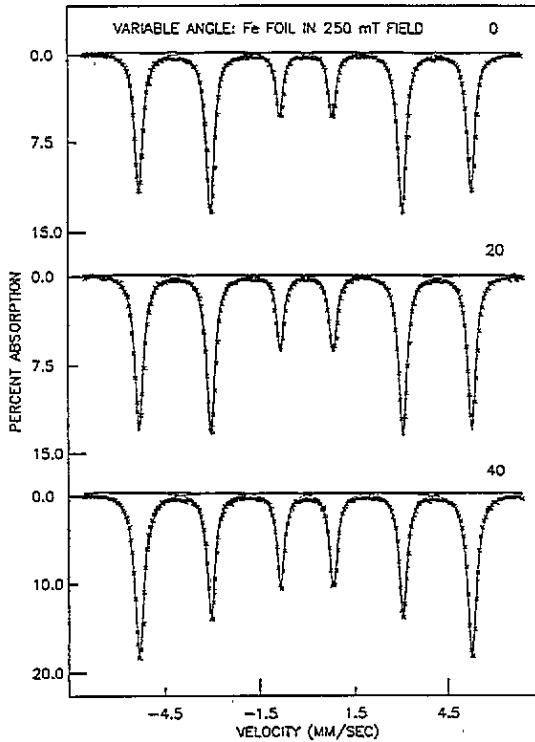
Figure 5. The room temperature Mössbauer spectra of a polycrystalline α-Fe foil subjected to an in-plane applied field of 250 mT along its y axis, and oriented with its normal (z axis) at $\psi = 0°$, 20° and 40° relative to an incident γ-ray beam in the yz-plane. The solid lines result from a least-squares fit using a constrained set of six Voigtian line profiles.
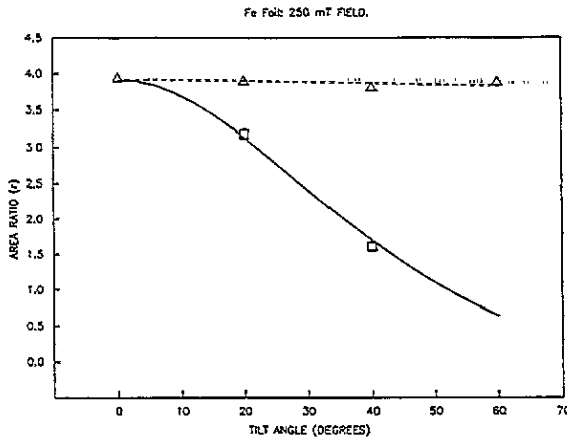

Figure 6. The relative area r of the second and fifth lines in the Mössbauer spectra of an α-Fe foil in an applied field of 250 mT, as a function of the angle of inclination between the γ-ray beam and the normal to the foil plane. The solid lines result from a least-squares fit using a double Gaussian moment distribution model.

annealed in a field of 0.4 T directed along the x axis for 20 min at 400 °C. This sample is denoted number 9 in table 1.
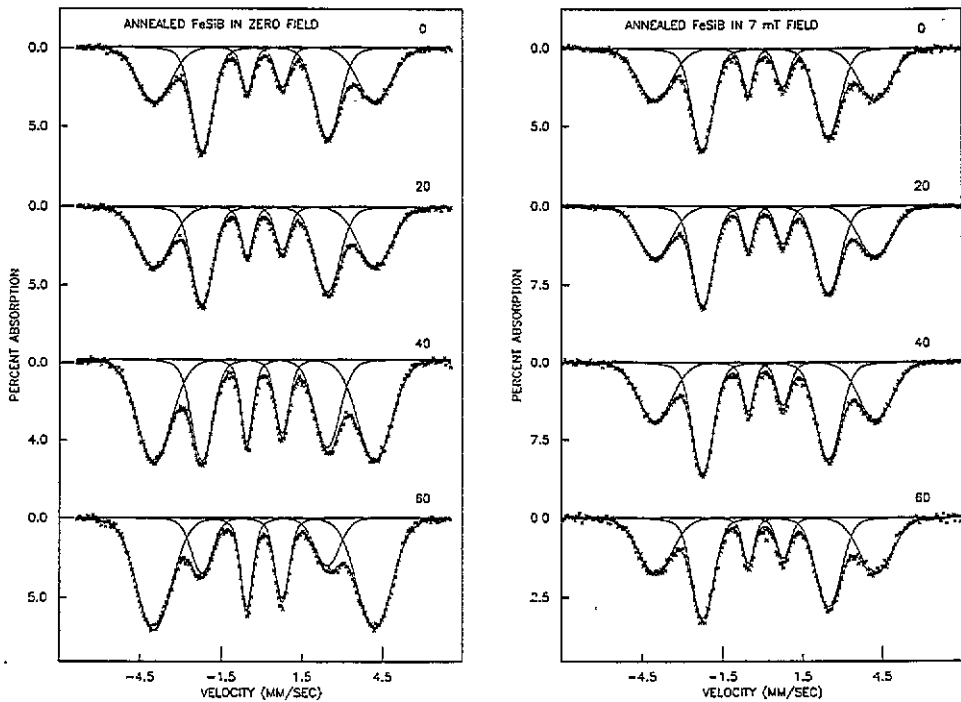
Figure 7. The room temperature Mössbauer spectra of sample 9, a $Fe_{78}Si_9B_{13}$ ribbon that was field annealed to induce magnetic anisotropy along its x axis prior to the experiment. Spectra are shown for (a) zero applied field and (b) an in-plane applied field of 50 mT directed along the y axis. In both cases the ribbon was oriented with its normal (z axis) at $\psi = 0°$, $20°$, $40°$ and $60°$ relative to an incident γ-ray beam in the xz plane. The change in the areas of the second and fifth lines reflects the reorientation of the Fe moments: away from the x axis in (a), and towards the applied field in (b). The solid lines result from a least-squares fit using a constrained set of six Voigtian line profiles.

Variable angle Mössbauer spectra were recorded both in zero field and with applied fields of 7 mT, 50 mT and 500 mT directed as near as possible to the y axis. Representative spectra for the zero field and 50 mT experiments are shown in figure 7. The results obtained for the area ratio parameter r for all four runs are shown in figure 8, along with the fits obtained using the double Gaussian model. The fitted parameters for the resultant moment distributions are listed in table 2.

Table 2. Out-of-plane (σ_u) and in-plane (σ_v) standard deviations for a double Gaussian distribution of moment directions, and the angles (u_0 and v_0) defining its central axis, for a field annealed $Fe_{78}Si_9B_{13}$ ribbon as a function of applied field. The field annealing induced a distribution centred on the ribbon's x axis (corresponding to $v_0 = 0°$). The applied field was directed along the y axis, corresponding to $v_0 = 90°$.

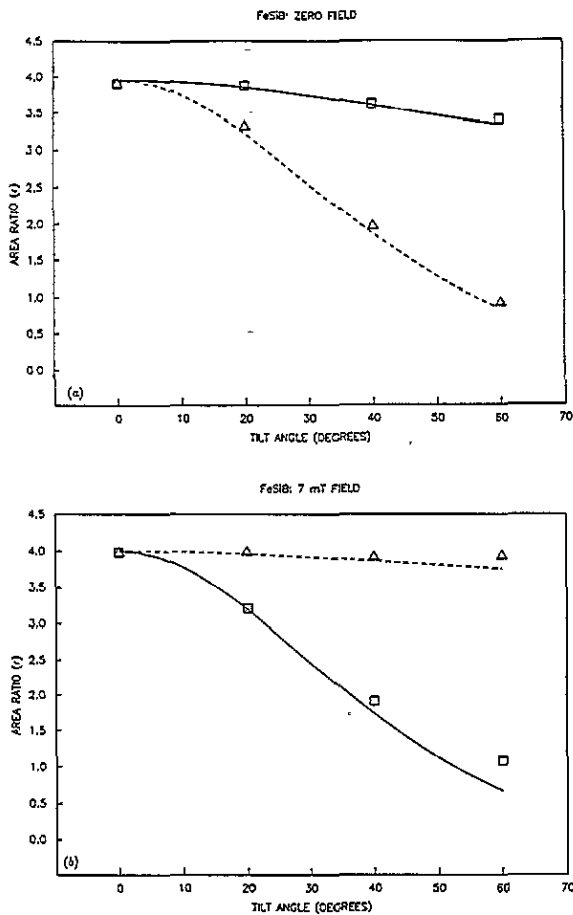| Applied field	u_0	v_0	σ_u	σ_v
None	$0°$	$0°$	$4.6° \pm 0.5°$	$21.4° \pm 0.3°$
7 mT	$0°$	$90°$	$0.0° \pm 0.5°$	$12.1° \pm 0.4°$
50 mT	$0°$	$90°$	$0.0° \pm 0.5°$	$12.8° \pm 0.4°$
500 mT	$0°$	$90°$	$0.0° \pm 0.5°$	$11.9° \pm 0.9°$

Figure 8. The relative area r of the second and fifth lines in the Mössbauer spectra of sample 9, a field annealed $Fe_{78}Si_9B_{13}$ ribbon, subjected to in-plane applied fields of 0, 7 mT, 50 mT and 500 mT. The parameter is shown as a function of the angle of inclination between the γ-ray beam and the normal to the foil plane. The solid lines result from a least-squares fit using a double Gaussian moment distribution model. The misfit apparent in the 500 mT graph is due to the out-of-plane component of the applied field, and is discussed in the text.

Table 3. Parameters defining an inverse sine distribution of moment directions for field annealed $Fe_{78}Si_9B_{13}$ ribbon as a function of applied magnetic field. The distribution is derived from the 'combed hair' model outlined in the text, defined in equation (10).

Applied field	$|u_{min}|$	u_{max}	$|v_{min}|$	v_{max}
None	$0° \pm 1°$	$24° \pm 4°$	$0° \pm 1°$	$83° \pm 6°$
7 mT	$0°$ [a]	$0°$ [a]	$0° \pm 1°$	$57° \pm 5°$
50 mT	$0°$ [a]	$0°$ [a]	$0° \pm 1°$	$48° \pm 5°$
500 mT	$0°$ [a]	$0°$ [a]	$0° \pm 1°$	$47° \pm 5°$

[a] Parameter fixed during fitting.

It is notable that for the 500 mT experiment the double Gaussian fit underestimated the value of r for the data points at inclination angles $\psi_{yz} = 20°$, 40° and 60°. However,
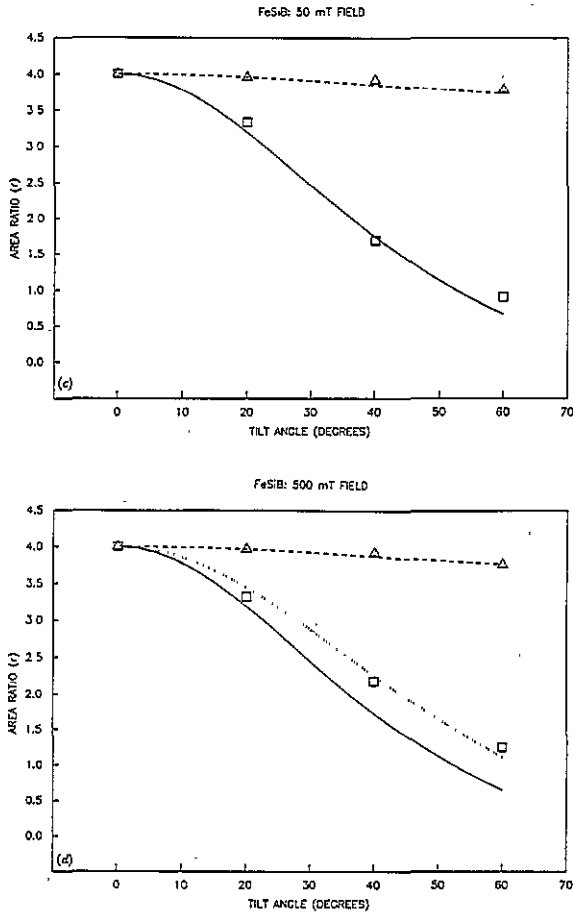
FeSiB: 50 mT FIELD

FeSiB: 500 mT FIELD

Figure 8. (Continued)

this is explicable as a result of the out-of-plane reorientation induced by the local magnetic flux no longer being in-plane in those spectra. (The corresponding spectra for the lower electromagnet fields of 7 mT and 50 mT show no sign of out-of-plane reorientation, indicating that in such low applied fields the magnetic flux is contained within the ribbon plane.) For the 500 mT spectra it was found that the difference between the measured and predicted values of r could be accounted for by allowing the symmetry axis of the double Gaussian distribution to rotate out-of-plane. It was assumed that the out-of-plane inclination angle u_0 of the symmetry axis scaled with the magnitude of the normal-to-plane component of the applied field. The dotted curve in figure 8 corresponds to $u_0 \cong 3.9°$, $7.3°$ and $9.8°$ for the $\psi_{yz} = 20°$, $40°$ and $60°$ spectra respectively.

On inspection of these data it is clear that the immediate effect of even the smallest 7 mT applied field is to collapse the moment distribution into the ribbon plane. However, once the moments lie in the ribbon plane, the in-plane distribution in direction is remarkably insensitive to the magnitude of applied field: the standard deviation is $\sim 12°$ for all three applied fields, 7 mT, 50 mT and 500 mT. This is an important clue to the origin of the moment canting in $Fe_{78}Si_9B_{13}$, supporting the notion that it is an intrinsic effect, some form of natural 'barrier'. Later we will present a model of moment canting originating

from frustrated exchange interactions between atoms (section 5). However, before that we consider the response of the material to even larger applied fields, up to 9 T, and test the degree to which the moment canting is impervious to applied field strength.

4. The response to normal-to-plane fields up to 9.0 T

4.1. The control experiment on α-Fe

In this section we consider the effect of the application of much larger magnetic fields directed normal to the ribbon plane. Once again it is instructive to test the experimental procedure with reference to the behaviour of polycrystalline α-Fe. The spectra shown in figure 9 were recorded with the α-Fe foil mounted inside either a 10 T or a 15 T superconducting magnet. Two features are noticeable in the spectra. The relative area r of the second and fifth lines in the six-line spectra is large in fields up to ~ 2 T, then falls to approximately zero in fields greater than ~ 3 T. Secondly, the magnitude of the magnetic hyperfine splitting of the spectra, reflected most clearly in the velocity separation of the first and sixth lines, is approximately constant in fields up to ~ 2 T, then begins to decrease systematically as the applied field increases. Both these features are emphasized in the graphs of r and hyperfine splitting as a function of applied field, shown in figure 10.

The change in the relative area r and in the magnetic splitting both convey information about the moment distribution in the foil. As has been discussed already, the change in r is related to the change in the angle α between the moments and the γ-ray beam. The change in magnetic splitting is also directly related to changes in α, since in this geometry the external applied field is parallel to the γ-ray beam. The 'effective' magnetic field experienced by an Fe atom in the foil is a vector sum:

$$B_{eff} = B_{hf} + B_0 + B_{dm} \tag{7}$$

where B_{hf} is the internal hyperfine field in α-Fe (of the order of 33.8 T at 4.2 K), B_0 is the applied field, and B_{dm} is the demagnetization field. It should be noted that the hyperfine field in Fe is dominated by core electron polarization, and is actually antiparallel to the Fe atomic moment. This therefore means that if the Fe atomic moments were completely aligned by the applied field, one would expect to see a linear *decrease* in B_{eff} as the applied field *increases*. This explains the behaviour seen in applied fields above ~ 2 T in figure 10.

The demagnetization field is given by $B_{dm} = -\mu_0 N M$, where N is the 'demagnetization factor' and M is the magnetization. For normal-to-plane magnetization $N \cong 1$, while for in-plane magnetization $N = 0$. Thus, for the normal-to-plane applied field experiment described here, the demagnetization field opposes the applied field. In fact the demagnetization field directly cancels out the effect of the applied field, $B_{dm} = -B_0$, until the magnetization induced by the applied field reaches its technical saturation value, M_s. At higher applied fields the magnetization is effectively constant, and the demagnetization field also remains constant. In α-Fe at 4.2 K, the field at which this transition takes place corresponds to $B_0 = \mu_0 M_s \cong 2.18$ T [32].

The predicted change in B_{eff} as a function of B_0 compares very favourably with the observed behaviour shown in figure 10. The effective field is constant up to $B_0 = 2.2 \pm 0.1$ T, after which it decreases roughly linearly with increasing applied field. The mean gradient over the region from $B_0 = 3$ T to 13 T region is -0.97 ± 0.02, although on careful inspection one finds that there is a slight curvature in the data, with the tangential slope of the curve approaching the limiting value of -1 as the applied field increases. This curvature is again understandable in terms of the approach to magnetic saturation in the
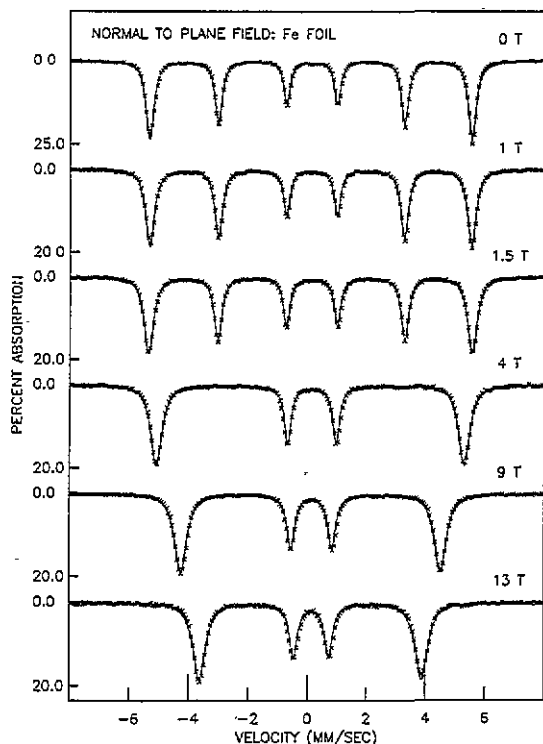
Figure 9. The Mössbauer spectra of a polycrystalline α-Fe foil at 4.2 K subjected to normal-to-plane applied fields of up to 13 T. The γ-ray beam was directed parallel to the applied field. Both the reduction in relative area of the second and fifth absorption lines, and the decrease in the splitting between the lines, are indicative of the Fe moments in the foil becoming aligned with the applied field. The solid lines are the results of a least-squares fit using a constrained set of six Voigtian line profiles.

foil, with the applied field competing against the magnetocrystalline and other anisotropies in the α-Fe grains. More details on this approach to saturation are afforded by the data on the relative area r as a function of field, which shows that up to $B_0 = 3$ T there is still an appreciable degree of resistance to the applied field, and that only for $B_0 \geqslant 4$ T does $r = 0$ (within experimental error), indicating that the Fe atomic moments are then completely collinear with the applied field.

Another notable feature in figure 10 is the enhancement in r for applied fields below ~ 2 T. At first sight this might seem unusual, as it indicates that the Fe moments are moving away from the applied field, to be oriented more closely in the ribbon plane, *perpendicular* to the applied field. However, such behaviour has been seen before in similar systems [33], and is understandable if one accepts that there is inevitably some degree of misalignment in the experiment, so that the applied field is not exactly normal to the α-Fe foil. Such a misalignment will produce an in-plane component of applied field. Although this in-plane component may be very small, the demagnetization field in the ribbon plane, as discussed above, is zero, so that the response of the foil magnetization to this field is uninhibited. Therefore, for applied fields up to the critical field of 2.18 T, a misalignment will preferentially produce in-plane reorientation of the Fe moments. We have tested this explanation of the observed enhancement in r by deliberately misaligning the ribbon-plane
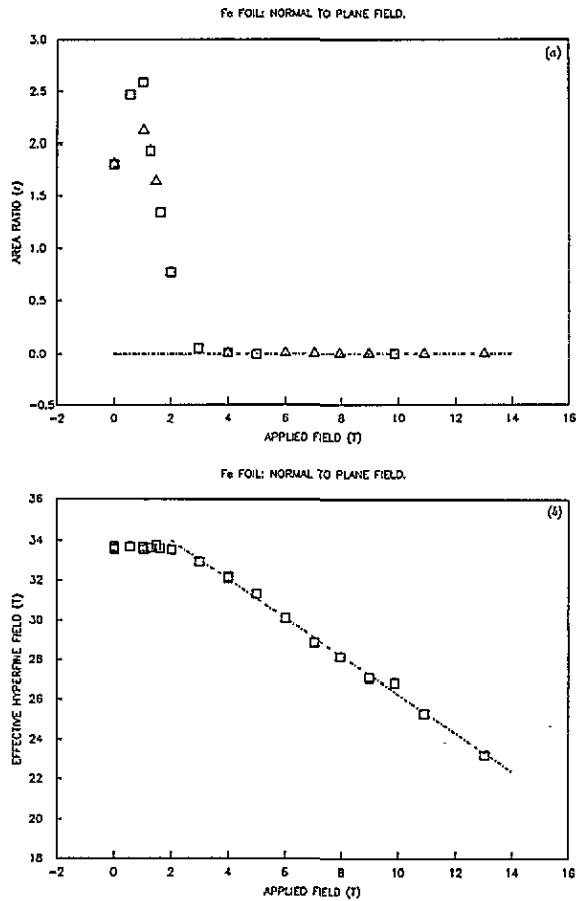
Fe FOIL: NORMAL TO PLANE FIELD.

Fe FOIL: NORMAL TO PLANE FIELD.

Figure 10. Data derived from the spectra of figure 8 for a polycrystalline α-Fe foil in normal-to-plane fields of up to 13 T: (*a*) the relative area r of the second and fifth lines in the spectra, and (*b*) the magnitude of the effective magnetic field experienced at the Fe nuclei, comprising the vector sum of the hyperfine, applied and demagnetization fields acting in the foil. The solid lines are a guide to the eye only.

normal to be $\sim 5°$ away from the applied field. As expected, the increase in r for $B_0 \leqslant 2.2$ T was then larger than in the first set of data.

4.2. FeSiB experiments

Normal-to-plane applied field spectra of a field annealed $Fe_{78}Si_9B_{13}$ specimen, sample 11, were recorded in a 10 T superconducting magnet for applied fields of 0, 1, 2, 3, 5 and 9 T. These spectra are shown in figure 11. In a similar manner to that observed in α-Fe, the relative area r of the second and fifth lines falls sharply with applied field, and the velocity separation of the outermost lines decreases in larger applied fields. Plots of both r and the effective field B_{eff}, as a function of B_0 are shown in figure 12. The plot of r versus B_0 differs from that observed in α-Fe in that it does not have a low-field maximum. This is partly because in the initial state the Fe moments lie near the ribbon plane ($r \cong 3.1$) whereas in α-Fe the initial state saw the Fe moments randomly oriented over a sphere ($r \cong 2.0$). It is also because the maximum demagnetization field in $Fe_{78}Si_9B_{13}$ is much smaller than in
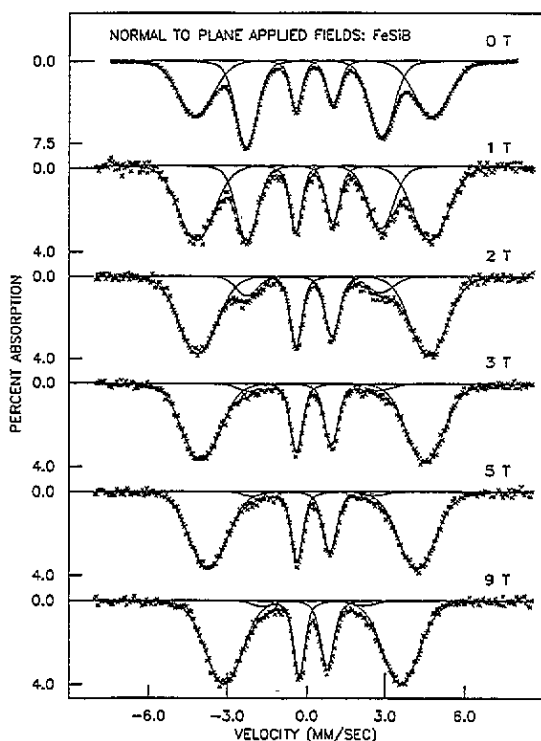
Figure 11. The Mössbauer spectra of sample 11, a field annealed $Fe_{78}Si_9B_{13}$ ribbon, at 4.2 K in normal-to-plane fields of up to 9 T. The γ-ray beam was directed parallel to the applied field. Both the reduction in relative area of the second and fifth absorption lines, and the decrease in the splitting between the lines, show the Fe moments in the foil becoming aligned with the applied field. The solid lines are the results of a least-squares fit using a constrained set of six Voigtian line profiles.

α-Fe, with $\mu_0 M_s$ in the metallic glass at 4.2 K falling well below the lowest experimental applied field of 1.0 T. The plot of B_{eff} versus B_0 is similar to that seen in α-Fe, with an initial flat region where the demagnetization field countermands the applied field, followed by a roughly linear decrease as the applied field penetrates the ribbon.

It is apparent in figures 11 and 12 that the relative areas of lines two and five in the Mössbauer spectra do not entirely fall to zero, even in a field of 9 T. This could be taken as evidence for moment canting, with $r \cong 0.13 \pm 0.02$ in the 9 T spectrum corresponding to a Gaussian distribution in moment directions with standard deviation $10.6° \pm 0.8°$. However, care should be taken in interpreting this result. Whereas in α-Fe the absorption lines were sharp and well-resolved, facilitating an accurate measurement of r, the $Fe_{78}Si_9B_{13}$ spectra of figure 11 have much broader lines, and the mean hyperfine splitting is somewhat smaller. This makes it more difficult to distinguish between a non-zero contribution of lines two and five and a possible contribution from the wings of lines one and six.

For this reason it is advisable to look for corroborating evidence from the field dependence of the effective hyperfine splitting. This is useful since the value of the effective field is well defined through the velocity separation of lines one and six. The slope of the curve of B_{eff} versus B_0 in the region with $B_0 \geqslant 3$ T is -0.95 ± 0.03. (Because of the limited number of datapoints collected the fitting uncertainty is relatively high.) If we assume that there is a mean angle of canting between the hyperfine field at the Fe nuclei and
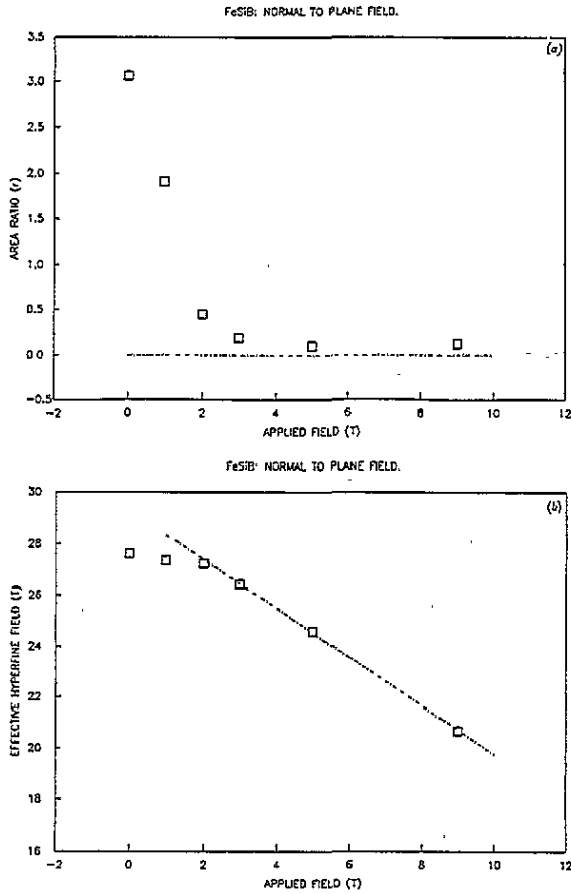
FeSiB: NORMAL TO PLANE FIELD.

FeSiB: NORMAL TO PLANE FIELD.

Figure 12. Data derived from the spectra of figure 10 for sample 11, a field annealed $Fe_{78}Si_9B_{13}$ ribbon, in normal-to-plane fields of up to 9 T: (a) the relative area r of the second and fifth lines in the spectra, and (b) the magnitude of the effective magnetic field experienced at the Fe nuclei, comprising the vector sum of the hyperfine, applied and demagnetization fields acting in the foil. The solid lines are a guide to the eye only.

the applied field which results in the nuclei seeing only 95% of the applied field strength, the required canting angle is $\langle\alpha\rangle = \cos^{-1}(0.95 \pm 0.03) = 18° \pm 6°$. This corresponds to a Gaussian distribution with a standard deviation $\sigma = 13° \pm 5°$. This is within experimental error of the figure estimated from the relative areas, and lends weight to the conclusion that there is substantial residual moment canting present in the ribbon even in the presence of normal-to-plane applied fields as large as 9 T.

Thus the in-plane and normal-to-plane applied field experiments yield very similar results: canting with $\sigma \sim 12°$ in 500 mT in-plane compared to $\sigma \sim 11°$ out-of-plane in 9 T. On the other hand, the in-plane applied fields were easily sufficient to achieve an out-of-plane $\sigma \sim 0°$. The implication is that co-operative effects such as demagnetization can relatively easily confine all the Fe moments to a planar state, but that there is some other mechanism which inhibits the complete collinear alignment of the Fe moments with an applied field. This mechanism appears to be intrinsic, as evidenced by its appearance in both the in-plane and normal-to-plane applied field experiments. It would also appear to
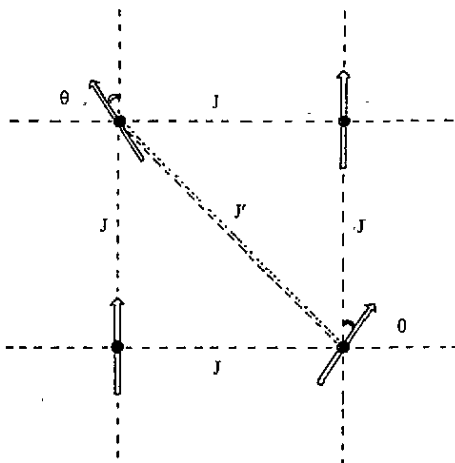
Figure 13. The theoretical basis of the 'combed hair' disturbed exchange model, illustrated for four atoms on a square lattice. The four nearest-neighbour exchange interactions are ferromagnetic, with exchange constant J. The next-nearest-neighbour interaction between two of the atoms is antiferromagnetic, with exchange constant J'. In the lowest energy state the two antiferromagnetically coupled moments are each canted by $\theta = \cos^{-1}(J/|J'|)$.

be not significantly affected by temperature. In the next section we discuss a model which may in part account for these observations.

5. 'Combed hair' model of moment canting due to disturbed exchange

To better understand and interpret quantitative data on the moment canting as a function of applied field, it is important that we consider what mechanisms might be giving rise to the canting. Although the double Gaussian moment distribution model that we have used so far is adequate for analysing the data, it is in essence a phenomenological model, without any atomic-scale justification. We present here the outline of an alternative *a priori* model of moment canting induced by frustrated exchange interactions. For reasons which will become obvious, we have termed this a 'combed hair' model of moment canting.

The starting proposition, given the fact that moment canting is seen to persist even in very large applied fields [5], is that the canting must be associated with exchange interactions rather than the much weaker anisotropic interactions. Secondly, on the basis of the topological disorder inherent in the system, we postulate that there may be some antiferromagnetic exchange interactions acting between some of the iron atoms. This is reasonable given that antiferromagnetic interactions are known to occur in appropriate geometries, as in the face-centred-cubic lattice of γ-Fe.

The effect of a few antiferromagnetic bonds on an isotropic ferromagnetic system is to induce frustration and local canting, and in turn to induce longer-range canting [11]. The first point is illustrated in the four-spin square lattice model illustrated in figure 13. Given ferromagnetic coupling between nearest-neighbour spins, with exchange constant $J > 0$, and a single antiferromagnetic interaction with $J' < 0$ between two of the next-nearest-neighbour spins, the energy of the system is $U(\theta) = -4J \cos \theta + |J'| \cos 2\theta$, where $\pm\theta$ is the canting angle of the antiferromagnetically-coupled spins. Equilibrium solutions for this are $\theta = 0$ and π, but also the canted state, where $|J'| > J$, of $\theta = \cos^{-1}(J/|J'|)$.

The second point regarding the effect that a few canted spins can have on the long-

range spin state is illustrated by imagining that the two canted spins are now placed within a large ferromagnetic region, as illustrated in figure 14. The spins neighbouring the two canted spins will experience a small exchange field directed perpendicular to the main ferromagnetic axis. We denote this field $h_x(r)$, where r is the position vector relative to the centre of the square lattice, midway between the two canted spins. Under the continuum approximation the magnetization due to this field may be written

$$M_x(r) = \int d^3r' \chi_{xx}(r - r') h_x(r') \tag{8a}$$

$$\chi_{xx}(r - r') = \sum_k \exp[ik \cdot (r - r')] \chi_{xx}(k) \tag{8b}$$

$$h_x(r') = J \sin\theta [\delta(r - b) - \delta(r + b)] \tag{8c}$$

where χ_{xx} is the magnetic susceptibility, $\delta(r \pm b)$ is the delta-function, and $b = \frac{1}{2}a(1, 1, 0)$ is the vector connecting the two canted spins, for a lattice constant a. In an isotropic magnet $\chi_{xx}(k)$ will vary as $(\Delta^2 + k^2)^{-1}$, where Δ^2 is the spin wave energy gap due to anisotropy and the external field, divided by the spin wave stiffness. Substituting this into (8), and making the approximation that $|r \pm b| \approx r \pm b \cdot \cos\phi$ where ϕ is the angle between the vectors r and b, we obtain

$$M_x(r, \phi) \propto (\exp[-|r - b|/\Delta]/|r - b|) - (\exp[-|r + b|/\Delta]/|r + b|) \tag{9a}$$

$$\propto 2r^{-1} \exp(-r/\Delta) \sinh(b \cos\phi/\Delta) + 2r^{-2} \exp(-r) b \cos\phi. \tag{9b}$$

The leading term in (9b) therefore shows that $M_x(r)$ varies as $\exp(-r/\Delta)/r$, *which is a very slow decay law*. Thus the effect of the pair of frustrated spins on the overall distribution of moment directions in the system may be large, as illustrated in figure 14. The resulting distribution may be visualized as resembling combed hair around a knot.
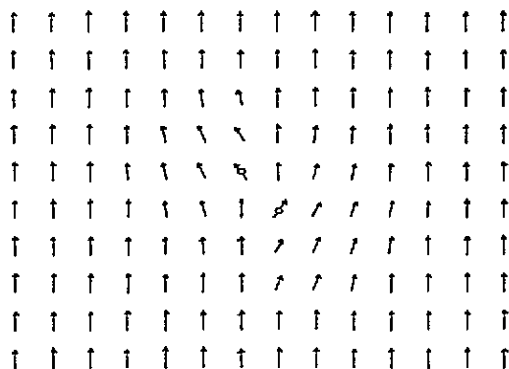
Figure 14. An illustration of long-range perturbations in moment direction around a pair of antiferromagnetically exchange coupled moments within a square lattice of ferromagnetically coupled moments, as determined in the 'combed hair' disturbed exchange model.

This model is very simple and requires refinement before it might realistically be said to model the random system of canting angles and interatomic separations in a metallic glass. Even so, an interesting result relating to the anticipated power-law behaviour of the probability distribution $P(M_x)$ may be obtained from the existing model, which is worth considering here. The pair of frustrated spins can be regarded as generating a dipolar disturbance in the system, which leads to $|M_x(r)| \propto r^{-2}$. At large distance the number of spins varies as r^2, so that we might expect $P(M_x)$ to vary as M_x^{-1}. A sketch of such a

distribution is shown in figure 15. There is a cut-off point for large M_x due to the finite canting angle caused by frustration, and for small M_x because there will be a finite mean distance separating pairs of frustrated spins.

The ramification of such a power law for $P(M_x)$ is that the probability distribution for the moment directions $P(u, v)$, previously modelled in equation (4) as a double Gaussian, might more properly be expressed as an inverse sine distribution:

$$P(u, v) = \text{constant} \qquad \text{for } u < u_{\min} \text{ and } v < v_{\min} \qquad (10a)$$

$$\propto (1/\sin u)(1/\sin v) \qquad \text{for } u_{\min} < u_{\max} \text{ and } v_{\min} < v < v_{\max} \qquad (10b)$$

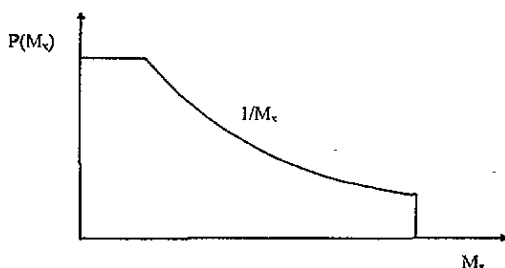$$= 0 \qquad \text{for } u > u_{\max} \text{ and } v > v_{\max}. \qquad (10c)$$

Figure 15. A schematic diagram of the inverse sine probability distribution of moment directions derived from the 'combed hair' disturbed exchange model.

We have analysed the applied field Mössbauer data for the FeSiB ribbons using this moment distribution. In the same way as for the double Gaussian, a computer program was written to evaluate a 500×500 equi-probable two-dimensional net in u and v. Results were obtained for the in-plane data that were identical in quality to those obtained with the double Gaussian model (figure 8): a full set of fitted parameters are given in table 3. In a field of 500 mT in-plane the distribution is characterized by $v_{\min} \approx 0°$ and $v_{\max} = 47° \pm 5°$. For the normal-to-plane applied field data, the figure $r = 0.13 \pm 0.02$ for the 9 T applied field corresponds to $u_{\min} = v_{\min} \approx 0°$ and $u_{\max} = v_{\max} = 62° \pm 6°$. Once again it is notable that the degree of in-plane canting seen at room temperature in fields up to 0.5 T is similar to the degree of out-of-plane canting found at 4.2 K in fields up to 9 T.

It is also significant that the inverse sine distribution gives good quality fits to the data. Not all models give good fits. In previous studies of as-cast, stress relieved and field annealed ribbons (in zero applied field) we found that models based on (i) a uniform moment, (ii) an ellipsoidal distribution, and (iii) a two-moment domain system, gave inferior fits compared to either a wedge-shaped or double Gaussian distribution [17, 19]. (The wedge-shaped model is a purely phenomenological model, as proposed by Melamud *et al* [6].) However, the unpolarized Mössbauer data in figure 8 is not sufficient to allow further differentiation between the three remaining candidate models. In a forthcoming paper on polarized Mössbauer studies of $Fe_{78}Si_9B_{13}$ we present data aimed at experimentally distinguishing between the wedge shaped, double Gaussian and inverse sine distributions [15]. But at this point, based on the available data, we cannot absolutely rule out any of the three possibilities, although it is clear that the wedge-shaped model is physically unlikely, and the inverse sine distribution, being based on an *a priori* model, is the most attractive.

6. Conclusions

In a series of unpolarized Mössbauer effect measurements on field annealed $Fe_{78}Si_9B_{13}$ ribbon, we have found that even in applied fields of up to 0.5 T in-plane and 9 T normal-to-plane, substantial moment canting persists. The magnitude of the canting is similar in both the 0.5 T and the 9 T data. We have considered an *a priori* model ascribing the origin of the canting to disturbed exchange interactions between some of the Fe moments. Taking as a first approximation a square plane lattice model, we have derived a quantitative description for the canting probability distribution: a truncated inverse sine distribution. The systematic variation in canting with applied field was found to be adequately described using this model, although a phenomenological double Gaussian model was equally able to fit the data. Polarized Mössbauer effect measurements are currently under way aimed at distinguishing experimentally between the inverse sine and double Gaussian distribution functions.

The body of evidence that has now been gathered, both in this work and in earlier polarized neutron, magnetostriction and high-field magnetization experiments, confirms that moment canting is an intrinsic property of some 3d-based amorphous alloys. The possible identification of this effect as due to a disturbed exchange mechanism between some of the magnetic atoms offers the potential for further work aimed at controlling or modifying the degree of frustration present, e.g. through varying preparation conditions, compositions and post-production treatment. If one could achieve an improved moment collinearity in moderate applied fields, the attendant increase in technical saturation magnetization could be a significant factor in future device development and manufacture. It is this prospect that is most likely to encourage further work in this field.

Acknowledgments

References

[1] Cowley R A, Patterson C, Cowlam N, Ivison P K, Martinez J and Cussen L D 1991 Non-collinear magnetic structures of Fe-based amorphous alloys *J. Phys.: Condens. Matter* **3** 9521–37
[2] Cowley R A, Cowlam N, Ivison P K and Martinez J 1992 The structure of Fe–Ni amorphous alloys *J. Magn. Magn. Mater.* **104–7** 159–60
[3] Bucholtz F, Koo K P, Dandridge A and Sigel G H Jr 1986 Easy axis distribution in transversely annealed Metglas 2605-S2 *J. Magn. Magn. Mater.* **54–7** 1607–8
[4] Thomas A P and Gibbs M R J 1992 Anisotropy and magnetostriction in metallic glasses *J. Magn. Magn. Mater.* **103** 97–110
[5] Graham C D and Gibbs M R J 1993 High-field magnetization of metallic glasses *IEEE Trans. Magn.* **29** 3458–60
[6] Melamud M, Swartzendruber L J, Bennett L H, Cullen J and Wun-Fogle M 1987 Moment distribution in amorphous magnetic ribbons by Mössbauer measurements *J. Appl. Phys.* **61** 3644–6
[7] Harker S J and Pollard R J 1989 Is iron-rich amorphous Fe-B asperomagnetic *J. Phys.: Condens. Matter* **1** 8269–73

[8] Pankhurst Q A, Betteridge S, Jiang J Z and Gibbs M R J 1994 In-plane moment canting in amorphous $Fe_{78}B_{13}Si_9$ in applied fields measured using polarized Mössbauer spectroscopy *IEEE Trans. Magn.* **30** 4809–11

[9] Gibbs M R J 1991 The effect of large spread in moment directions on anisotropy and magnetostriction in amorphous alloys *Proc. 5th Int. Conf. Physics of Magnetic Materials (Madralin, Poland, 1990)* ed W Gorzkowski, M Gutowski, H K Lachowicz and H Szymczak (London: World Scientific) pp 242–58

[10] Fähnle M, Furthmüller J, Pawellek R, Beuerle T and Elsässer C 1991 Magnetostriction in amorphous ferromagnets: theory and interpretation of experiments *Proc. 5th Int. Conf. Physics of Magnetic Materials (Madralin, Poland, 1990)* ed W Gorzkowski, M Gutowski, H K Lachowicz and H Szymczak (London: World Scientific) pp 204–41

[11] Villain J 1979 Insulating spin glasses *Z. Phys.* B **33** 31–42

[12] Chikazumi S 1993 Disturbed exchange model, unpublished

[13] Liebs M, Hummler K and Fähnle M 1994 Influence of structural disorder on the magnetic order—an *ab initio* study of amorphous Fe, Co and Ni, unpublished

[14] Lorenz R and Hafner J 1995 Non-collinear spin-structures in amorphous iron and iron-based alloys *J. Magn. Magn. Mater.* **139** 209–27

[15] Pankhurst Q A, Betteridge S, Jiang J Z, Gibbs M R J, Jäschke J, Rüter H D and Gerdau E 1995 Moment canting in amorphous FeSiB ribbons in applied fields: polarised Mössbauer effect studies, unpublished

[16] Pankhurst Q A, Gibbs M R J and Thomas A P 1992 Moment distribution in $Fe_{78}B_{13}Si_9$ ribbons by Mössbauer spectroscopy *J. Magn. Magn. Mater.* **104–7** 111–2

[17] Pankhurst Q A and Gibbs M R J 1993 Moment canting in 3d-based amorphous ferromagnets *J. Phys.: Condens. Matter* **5** 3275–88

[18] Pankhurst Q A, McCammon C A and Gibbs M R J 1993 Moment canting in metallic glass ribbons using spatially resolved Mössbauer spectroscopy *IEEE Trans. Magn.* **29** 3460–2

[19] Jiang J Z, Pankhurst Q A and Gibbs M R J 1994 A double Gaussian approach to the moment distribution in amorphous metals *Hyperfine Interact.* **94** 2137–43

[20] Jiang J Z, Pankhurst Q A and Gibbs M R J 1995 The effect of field annealing on moment canting in amorphous $Fe_{78}Si_9B_{13}$ *J. Magn. Magn. Mater.* **140–4** 323–4

[21] Vandenberghe R E, Gryffroy D and De Grave E 1987 On the analysis of Mössbauer spectra of metallic glasses *Nucl. Instrum. Methods Phys. Res.* B **26** 603–9

[22] Window B 1971 Hyperfine field distributions from Mössbauer spectra *J. Phys. E: Sci. Instrum.* **4** 401–2

[23] Hesse J and Rübartsch A 1974 Model independent evaluation of overlapped Mössbauer spectra *J. Phys. E: Sci. Instrum.* **7** 526–32

[24] Lines M E and Eibschütz M 1983 Correlation effects in the Mössbauer spectra of amorphous metallic magnetic materials *Solid State Commun.* **45** 435–9

[25] Bhatnagar A K and Ravi N 1983 Magnetic properties of a glassy ferromagnet $Fe_{78}B_{13}Si_9$ *Phys. Rev.* B **28** 359–67

[26] Dunlap R A and Ritcey S P 1985 Comment on 'Magnetic properties of a glassy ferromagnet: $Fe_{78}B_{13}Si_9$' *Phys. Rev.* B **32** 3325–7

[27] Vincze I 1978 Evaluation of complex Mössbauer spectra in amorphous and crystalline ferromagnets *Solid State Commun.* **25** 689–93

[28] Chien C L 1981 Comments on the analysis of hyperfine field distributions in amorphous magnetic solids using a spectrum subtraction method *Phys. Rev.* B **23** 4788–90

[29] Margulies S and Ehrman J R 1961 Transmission and line broadening of resonance radiation incident on a resonance absorber *Nucl. Instrum. Methods* **12** 131–7

[30] Hollatz R, Gerdau E and Rüffer R 1986 Field distributions at ^{57}Fe in Zn_2-Y and their fitting with the transmission integral *Hyperfine Interact.* **28** 807–10

[31] Shirley D A, Kaplan M and Axel P 1961 Recoil-free resonant absorption in Au^{197} *Phys. Rev.* B **123** 816–30

[32] Bozorth R M 1951 *Ferromagnetism* (New York: Van Nostrand) p 581

[33] Gonser U 1981 Mössbauer spectroscopy on amorphous metals *Atomic Energy Review Suppl. No. 1: Application of Nuclear Techniques to the Studies of Amorphous Metals* ed U Gonser (Vienna: International Atomic Energy Review Agency) pp 203–28